ACS Energy LETTERS

Cite This: ACS Energy Lett. 2018, 3, 264−269

LETTER

# Electrochemical Lithium Doping Induced Property Changes In Halide Perovskite $CsPbBr_3$ Crystal

Qinglong Jiang,[†] Xiaoqiao Zeng,[‡] Ning Wang,[*,⊥,∥] Zhili Xiao,[†] Zhanhu Guo,[*,§] and Jun Lu[*,‡]

[†]Materials Science Division, Argonne National Laboratory, Lemont, Illinois 60439, United States

[‡]Chemical Sciences and Engineering Division, Argonne National Laboratory, Lemont, Illinois 60439, United States

[§]Department of Chemical and Biomolecular Engineering, University of Tennessee, Knoxville, Tennessee 37996, United States

[∥]School of Material Science and Engineering, Jiangsu University of Science and Technology, No. 2, Mengxi Road, Zhenjiang 212003, Jiangsu P. R. China

[⊥]State Key Laboratory of Marine Resource Utilization in South China Sea, Hainan University, Haikou 570228, P.R. China

Supporting Information

**ABSTRACT:** **Electrochemical doping was used to dope lithium into perovskite $CsPbBr_3$ crystal. Due to the doping, diamagnetic behavior was observed with a transition temperature ($T_c$) of 7.17 K. Burstein−Moss effect related photoluminescence (PL) blue-shift was observed as long as 15 nm. UV−vis-NIR spectra indicate that the absorption has been enhanced. The doped $CsPbBr_3$ crystal generated 8 nA photocurrent, which is higher than the undoped $CsPbBr_3$ crystal.**

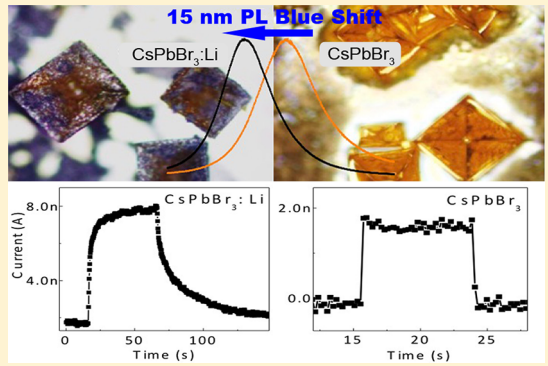


With over 20% energy conversion efficiency achieved in a short time, halide perovskite materials $MPbX_3$ ($M = CH_3NH_3^+$, $Cs^+$, $FA^+$, or mixture; $X = I^-$, $Br^-$, $Cl^-$, $SCN^-$, or mixture) become the most promising material for the next generation of solar cells.[1−10] The focused researches are halide perovskite materials containing iodine ($MPbI_3$) due to their light absorption is up to 800 nm,[2] which corresponding to high light utilization and high photocurrent. Although the photostability of bromide compounds are better than iodine compounds, the light absorption for bromide perovskite materials ($MPbBr_3$) is only up to 550 nm,[11,12] which extremely limited the light utilization for solar cells.

Dopants, introduced impurities in material, can strongly modify electronic, optical, and other properties of materials.[13,14] So far, the reported dopants for halide perovskite materials ($MPbX_3$) include: doped Bi can be used to tune the band gap (band gap narrowing, BGN) and enhance the electrical conductivity of $MAPbBr_3$ by $10^4$ fold;[15] Al n-doping can improve crystal quality and microstrain of halide perovskite, which in turn improve the efficiency of solar cells;[16] n-type doping by Sb elevates the quasi-Fermi energy level of the halide perovskite and promotes electron transport in the working solar cell.[17] All of the reported halide perovskite doping literatures are in situ synthesis method. As one of the doping methods, electrochemical doping is a simple and easy way to manage the properties of target materials.[18]

Earlier, we reported that lithium doped halide perovskite $CsPbBr_3$ crystal enhanced the light emitting in LEDs with low turn-on voltage.[18] The lithium doping or intercalation related halide perovskite attracted more and more attention.[19,20] We further found the diamagnetic behavior, PL blue-shift, and enhanced photocurrent behavior in the lithium doped $CsPbBr_3$ crystals. The lithium ex situ doping levels of perovskite $CsPbBr_3$ crystals can be controlled electrochemically by adjusting the doping voltage or time without destroying the crystal structure, which in turn causes $Pb^{2+}$ reduction related diamagnetism and doping level related Burstein−Moss PL blue-shift. Meanwhile, the optical-electric properties of $CsPbBr_3$ perovskite crystals were changed to absorb more light. Correspondingly, the doped black $CsPbBr_3$ crystals generated higher $V_{oc}$ and higher photocurrent as a photovoltaic material compared with the orange color undoped crystals.

**Received:** December 6, 2017
**Accepted:** December 29, 2017
**Published:** December 29, 2017




DOI: 10.1021/acsenergylett.7b01230
ACS Energy Lett. 2018, 3, 264−269

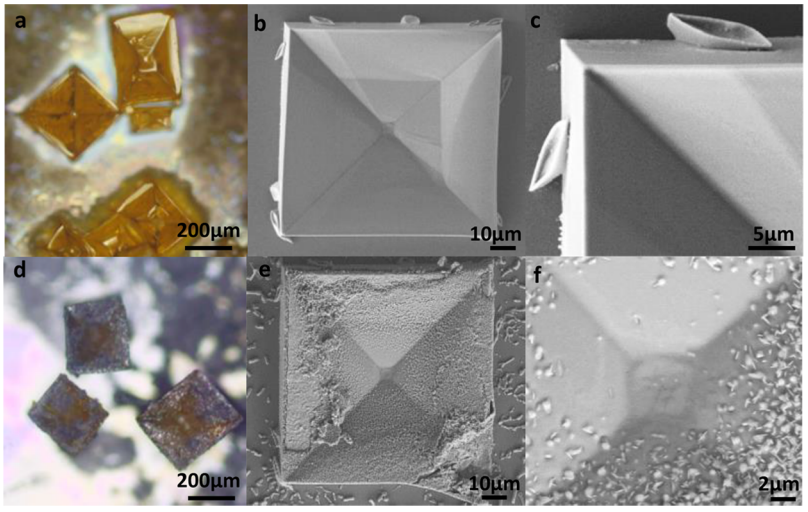


**Figure 1. Optical (a,d) images of undoped and lithium doped $CsPbBr_3$ crystal. (b,e) SEM images of the same single crystal before and after doping. (c,f) Zoomed in SEM images.**

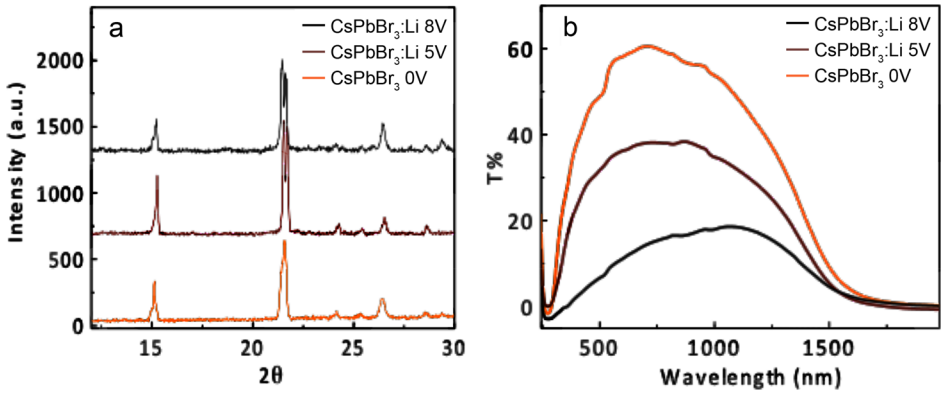


**Figure 2. (a) XRD of original $CsPbBr_3$ and lithium doped crystal. (b) Electrical-optical change of $CsPbBr_3$ perovskite: UV−vis-NIR spectra before and after lithium ion doping with $LiClO_4$ as electrolytes.**

Because of the lithium doping, the color changes of crystals can be clearly seen from the optical images in Figure 1a,d. Additional optical images for color changed crystal (different doping levels) can be found in Supporting Information, Figure S1a−S1d. With 1 M $LiClO_4$ in diethyl carbonate as electrolytes, 2 V or lower doping voltage in 30 s cannot cause visible color change; visible color change can be seen when the voltage is over 3 V. Both doping voltage over 10 V and doping time over 60 s cause damage to the crystals. Usually, the bottom of the crystal will be doped at the beginning due to better contact with electrode and lower resistance. SEM images in Figure 1b,e compared the surface morphology changes of the same crystal after lithium doping. Figure 1c,f are the zoomed in SEM images of the same crystal that show the difference of surface morphology in detail.

The doped $CsPbBr_3$ perovskite crystals are stable in the inert environment for months. The black $CsPbBr_3$ crystals turned into white after exposure to air which related to the humidity of the air. Optical images in Figure S1d−S1f in Supporting Information shows the color of crystals changing from black into white after exposure to moisture. The undoped part of the crystal remains unchanged, shown as the orange color on the crystal in Supporting Information, Figure S1f.

X-ray powder diffraction (XRD) indicates there is no structure damage for halide perovskite $CsPbBr_3$ during the doping. Figure 2a shows the $CsPbBr_3$ diffraction patterns at different applied voltages. The bottom pattern is the original $CsPbBr_3$ material. As the applied voltage increases, no major change of XRD pattern can be observed, indicating no major change of perovskite crystal structures after lithium was electrochemically doped into the $CsPbBr_3$ crystal. These characteristic peaks disappear only when the applied voltage is extremely high as shown in Supporting Information, Figure S2.

To investigate the color change of lithium doped crystal, the UV−vis-NIR spectra measurement (transmission) results are shown in Figure 2b. To get accurate UV−vis-NIR spectra on the same spot, $CsPbBr_3$ precursor was mixed with solution of PEO (polyethylene oxide) in DMSO in which the colored state could last for a longer time even when voltage was removed. The original $CsPbBr_3$ has absorption edge at 540 nm, with over 40% transmittance between 400 and 1200 nm (maximum of 60% at 700 nm). The maximum transmittance decreases to 38% at an applied voltage of 5 V and keeps decreasing to less than 20% when the voltage increases to 8 V. Apparently, the doping enhances the light absorption. It can be attributed to low-energy photon and/or thermal excitation of trapped electrons in localized states of the defects. Excess doping and impurity caused band gap narrowing (BGN).[21] Illustration of BGN was listed as Figure S4b in Supporting



DOI: 10.1021/acsenergylett.7b01230
ACS Energy Lett. 2018, 3, 264−269

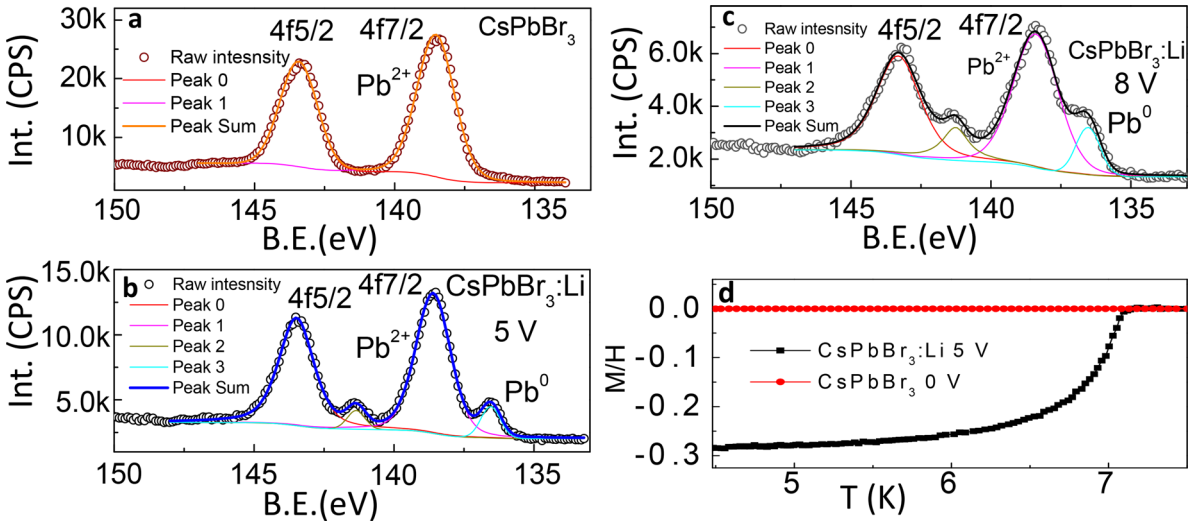


**Figure 3. X-ray photoelectron spectroscopy (XPS) and temperature (T) dependence of the magnetization $M(T)$ of $CsPbBr_3$:Li. (a) $CsPbBr_3$. (b) doped at 5 V. (c) doped at 8 V. (d) T(K) vs $M(T)$.**

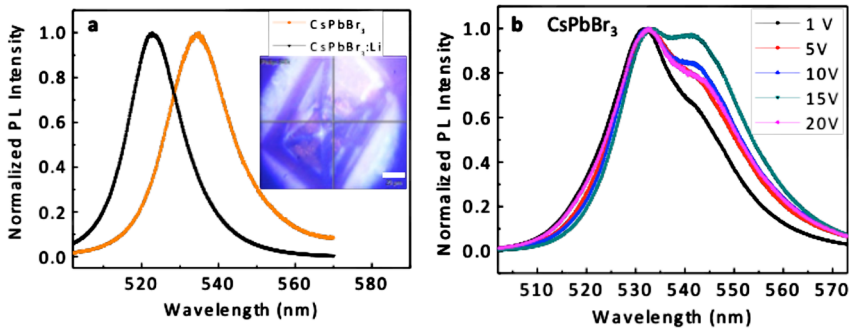


**Figure 4. (a) Photoluminescence of both doped and undoped $CsPbBr_3$ crystal, the scale bar of the crystal picture is 20 $\mu$m. (b) PL under different voltages for the undoped $CsPbBr_3$ crystal.**

Information. Similar results of light absorption enhancement and band gap narrowing have also been observed in N-doped $TiO_2$[22] and Ru-doped $TiO_2$.[21]

X-ray photoelectron spectroscopy (XPS), cyclic voltammetry (CV), and magnetization measurement were carried out to investigate the doped $CsPbBr_3$ perovskite. We futhure analyzed the results of XPS for Pb as shown in Figure 3. In Figure 3a, the main pair of peaks due to the Pb $4f_{7/2}$ and Pb $4f_{5/2}$ is found at around 138.5 and 143.4 eV, respectively, which corresponds to the $2^+$ oxidation state of Pb.[23] In Figure 3b, an additional pair of peaks is found at 141.4 and 136.5 eV in the lithium doped sample at an applied voltage of 5 V, which are attributed to zero oxidation state of $Pb^0$. Most likely, the reduction of $Pb^{2+}$ can be attributed to the negative bias voltage. As the applied voltage increased to 8 V as shown in Figure 3c, the ratio between peak 143.4 eV ($Pb^{2+}$) and 141.3 eV ($Pb^0$) decreased from 13.9 to 4.0, indicating that more $Pb^{2+}$ has been reduced at higher applied voltage. The detailed data is listed in the Supporting Information as Table S1. CV is shown in Supporting Information Figure S3. In the eight CV cycles, a cathodic peak from $Pb^0/Pb^{2+}$ was observed at 0.44 V when scan $CsPbBr_3$ material vs saturated calomel electrode (SCE). No major current and peak changes can be observed.

In Figure 3d, the magnetization measurement result of lithium doped $CsPbBr_3$ was presented. The doped $CsPbBr_3$ sample was collected from FTO glass and cooled down in zero applied field. A desired value a magnetic field was applied and the magnetization was measured as a function of temperature upon warming. Lithium doped $CsPbBr_3$ shows a transition temperature ($T_c$) at about 7.17 K, which is the same as Pb metal.[24] No $T_c$ was detected when doping voltage is 0 V (red line in Figure 3d). This result shows that $CsPbBr_3$ can be turned into diamagnetic material by lithium doping, which also further proves the reduction of $Pb^{2+}$ to $Pb^0$.

Photoluminescence (PL) measurement was carried out to invistigate the doping of $CsPbBr_3$. In Figure 4a, the inset is the optical image of the tested doped crystal. Because of the doping, $CsPbBr_3$ perovskite material shows the Burstein−Moss effect induced PL blue-shift as long as 15 nm (or 0.067 eV) under laser light excitation from 535 nm for the undoped $CsPbBr_3$ crystal to 520 nm for the deeply doped crystal. As the doping level increased, electrons populate states within the conduction band (CB) due to Burstein−Moss (BM) effect, which elevates the Fermi level higher to the CB. According to the electrhochemistry result,[18] about three lithium ions can be doped in the $CsPbBr_3$ crystal, which indicates a deep doping. The result is similar to dopant Sb elevating the Fermi energy level of the halide perovskite.[17] Because Pauli's exclusion principle forbids excitation into occupied states, electrons from the top of the valence band can only be excited into the conduction band above the Fermi level.[25] Band tailoring might occur due to doping, which enhance the absorption. B−M band filling caused the PL blue-shift. The Illustration is shown in Supporting Information, Figure S4b. More PL of other


DOI: 10.1021/acsenergylett.7b01230
ACS Energy Lett. 2018, 3, 264−269

undoped $CsPbBr_3$ crystal and different lithium doped crystals can be found in Supporting Information, Figure S4c. Similar result of Bi heavily doped halide perovskite $CsPbBr_3$ was reported with 5 nm Burstein−Moss blue-shift.[26] The difference is that Bi doping is in situ and substitutional, while smaller lithium doping is interstitial and doping level can be higher followed by the reduction of Pb. Most likely, the doped Li remains the valence +1 to keep the charge balance, which could be the reason for the unique properties.

It has been reported that external stimulations can cause the properties changes of halide perovskite materials. For example, external light illumination can cause redistribution and self-poling of the halide perovskite material.[27,28] To confirm that the PL blue-shift is doping related other than caused by electric field, PL of undoped $CsPbBr_3$ crystal under different voltages of applied electric field was measured. In Figure 4b, the PL of the $CsPbBr_3$ crystal under different applied voltages without lithium doping shows a new shoulder peak at 540 nm. The major peak at around 535 nm is from the $CsPbBr_3$ crystal. As 1 V of bias voltage was applied, a shoulder PL peak showed up. The intensity of this shoulder peak increases as the applied voltage increases and reaches almost the same intensity of the peak at 535 nm at 15 V. When the applied voltage reaches 20 V, the intensity drops, which is most likely due to the breakdown of the electric field induced p−i−n structure in the halide perovskite material.[11] It has been reported that PL changes for p type and n type doped material even in the same sample at different p or n regions.[25] Most likely, the new PL peak is caused by the applied external electric field, which is similar to the reversible and light-induced transformations.[29] These results indicate that the PL blue-shift of the doped $CsPbBr_3$ crystal is related to doping other than the external electric field.

It is known that halide perovskite materials are sensitive to light, which can be used as solar cells and light sensors.[30] The time dependent photocurrent of the undoped and doped $CsPbBr_3$ crystal under white light was investigated. As shown in Figure 5, photocurrent is almost 4 times higher for doped (darkened) $CsPbBr_3$ crystal than the undoped orange crystal, which is similar to the stronger light response for N-doped red $TiO_2$ than the undoped white $TiO_2$.[22] For the undoped $CsPbBr_3$ crystal in Figure 5a, it costs less than 0.5 s for the photocurrent to reach the maximum (light on) and decay to zero (light off). While in the case of doped $CsPbBr_3$ crystal in Figure 5b, it costs more than 25 s to reach 95% of the maximum and over 100 s to decay. Higher baseline in Figure 5b is due to the imcomplete discharge before the light turned on. It has been reported that lithium dopants cause deep electron traps in semiconductor, such as ZnO, which in turn affects the carrier diffusion length and lifetime.[31] It is also known that defects affect the photoresponse speed of semiconductor.[32] In this case, the doped lithium played the same role as defect centers and traps. The lithium ion battery research indicates that more than one lithium ions can be inserted into the unit cell of halide perovskite $CH_3NH_3PbBr_3$.[20] In this case, the lithium should remain in a valence of +1 to keep charge balance due to reduction of $Pb^{2+}$, which becomes trap states in $CsPbBr_3$ as shown in Supporting Information, Figure S4a, and Figure 4b. There are options for the exitons: through indirect trapping states hop (low energy excitions, red line in Figure S4b) or direct conduction band jump (high energy excitions). As a result, photocurrent rising transient was delayed in Figure 5b. Once the light was turned off, the combination started immediately in the undoped $CsPbBr_3$ crystal, which is the reason for fast decay in Figure 5a. In the case of doped crystal when light is off, the combination is delayed by doping centers, which probably results in a stable photocurrent. Again, this result is similar to the long-time photocurrent stability of N-doped $TiO_2$.[22] More time dependent photocurrent of various undoped and doped $CsPbBr_3$ crystals can be found in Supporting Information, Figure S5. We also noticed that other halide perovskite materials in a large area has similar photon response behavior. Supporting Information, Figure S6, shows the current vs time photon response of halide perovskite $(CH_3NH_3)_2Pb(SCN)_2I$, and other investigations of this material was carried out in a different project.

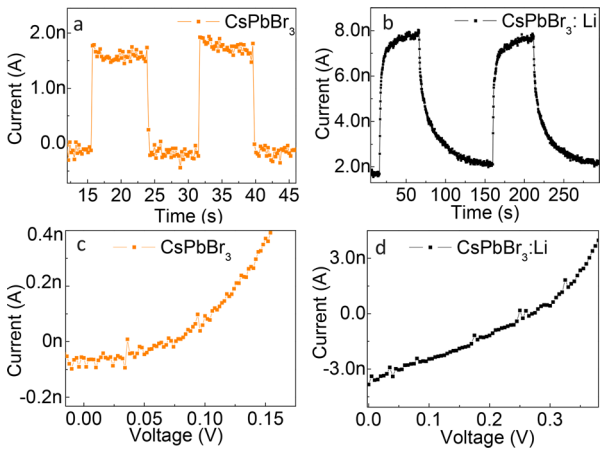


**Figure 5. (a,b) Current vs time of undoped and lithium doped $CsPbBr_3$ crystal. (c,d) $I-V$ curve of undoped and lithium doped $CsPbBr_3$ crystal.**

Halide perovskite solar cells can work without hole transport material (HTM).[33,34] Current−voltage ($I-V$) curves measured directly on crystals are compared in Figure 5c,d. The undoped $CsPbBr_3$ crystal gave very low photocurrent and 68 mV $V_{oc}$ for the tested sample. It is worth noting that the test was carried out on $\mu$m size crystals instead of a large area of material. With the same testing condition, the doped $CsPbBr_3$ crystal has much higher photocurrent and $V_{oc}$, which are 3.93 nA and 280 mV, respectively. This result is accordance with the increase of $V_{oc}$ for in situ Sb doped $CH_3NH_3PbI_3$ perovskite due to the doping related elevation of the quasi-Fermi level.[17] The difference is that the in situ doped Sb decreases the utilization of light (color changed from black to orange, photocurrent deceased correspondingly), while the ex situ doping of lithium increases the utilization of light (color changed from orange to black, photocurrent increased correspondingly). The doped $CsPbBr_3$ crystal has a deeper color, which obviously can utilize more light than the undoped orange color $CsPbBr_3$ crystal. More $I-V$ curves for various lithium doped crystals can be found in Supporting Information, Figure S7. The photovoltaic behaviors for different crystals are more likely dependent on the doping levels, in other words, the light absorption level of the doped crystals. The doped $CsPbBr_3$ (darkened) crystals apparently can increase the utility of light, which in turn improve the photovoltaic performance.

In summary, we further explore the properties for the lithium doped $CsPbBr_3$ perovskite. We found diamagnetism for the doped $CsPbBr_3$ perovskite with a $T_c$ of 7.17 K. The


DOI: 10.1021/acsenergylett.7b01230
ACS Energy Lett. 2018, 3, 264−269

doping related Burstein−Moss effect caused PL blue-shift was observed as long as 15 nm. Absorption of light has been enhanced. Photovoltage and photocurrent test results indicate that the lithium doped $CsPbBr_3$ perovskite can improve the performance as photovoltaic material. Further study will be carried out for other halide perovskite materials ($MPbX_3$). These new findings are expected to open new research areas in diamagnetism and improve the performance of perovskite solar cells in the future.

## ■ ASSOCIATED CONTENT

### Supporting Information

The Supporting Information is available free of charge on the ACS Publications website at DOI: 10.1021/acsenergylett.7b01230.

Experimental section, SEM, XPS table, CV, PL, current vs time, $I-V$ curve (PDF)

## ■ AUTHOR INFORMATION


### Corresponding Authors

*J.L.: E-mail, junlu@anl.gov.
*Z.G.: E-mail, zguo10@utk.edu.
*N.W.: E-mail, wangn02@foxmail.com.

### ORCID

Zhili Xiao: 0000-0001-8012-2814
Zhanhu Guo: 0000-0003-0134-0210
Jun Lu: 0000-0003-0858-8577


### Notes

The authors declare no competing financial interest.

## ■ ACKNOWLEDGMENTS

We acknowledge the theoretic support from Dr. Mingming Chen and Dr. Junqiang Li. J.L. gratefully acknowledges support from the U.S. Department of Energy (DOE), Office of Energy Efficiency and Renewable Energy, Vehicle Technologies Office. Argonne National Laboratory is operated for DOE Office of Science by UChicago Argonne, LLC, under contract number DE-AC02-06CH11357.

## ■ REFERENCES


(1) Yang, W. S.; Noh, J. H.; Jeon, N. J.; Kim, Y. C.; Ryu, S.; Seo, J.; Seok, S. I. High-Performance Photovoltaic Perovskite Layers Fabricated through Intramolecular Exchange. *Science* **2015**, *348* (6240), 1234−1237.

(2) Jiang, Q.; Rebollar, D.; Gong, J.; Piacentino, E. L.; Zheng, C.; Xu, T. Pseudohalide-Induced Moisture Tolerance in Perovskite $CH_3NH_3Pb(SCN)_2I$ Thin Films. *Angew. Chem., Int. Ed.* **2015**, *54* (26), 7617−7620.

(3) You, J.; Meng, L.; Song, T.-B.; Guo, T.-F.; Yang, Y. M.; Chang, W.-H.; Hong, Z.; Chen, H.; Zhou, H.; Chen, Q.; Liu, Y.; De Marco, N.; Yang, Y.; et al. Improved Air Stability of Perovskite Solar Cells via Solution-Processed Metal Oxide Transport Layers. *Nat. Nanotechnol.* **2016**, *11* (1), 75−81.

(4) Mei, A.; Li, X.; Liu, L.; Ku, Z.; Liu, T.; Rong, Y.; Xu, M.; Hu, M.; Chen, J.; Yang, Y.; et al. A Hole-Conductor−Free, Fully Printable Mesoscopic Perovskite Solar Cell with High Stability. *Science* **2014**, *345* (6194), 295−298.

(5) Jiang, Q.; Sheng, X.; Li, Y.; Feng, X.; Xu, T. Rutile $TiO_2$ Nanowire-Based Perovskite Solar Cells. *Chem. Commun.* **2014**, *50* (94), 14720−14723.

(6) Jiang, Q.; Sheng, X.; Shi, B.; Feng, X.; Xu, T. Nickel-Cathoded Perovskite Solar Cells. *J. Phys. Chem. C* **2014**, *118* (45), 25878−25883.

(7) Burschka, J.; Pellet, N.; Moon, S.-J.; Humphry-Baker, R.; Gao, P.; Nazeeruddin, M. K.; Grätzel, M. Sequential Deposition as a Route to High-Performance Perovskite-Sensitized Solar Cells. *Nature* **2013**, *499* (7458), 316−319.

(8) Jeon, N. J.; Noh, J. H.; Yang, W. S.; Kim, Y. C.; Ryu, S.; Seo, J.; Seok, S. I. Compositional Engineering of Perovskite Materials for High-Performance Solar Cells. *Nature* **2015**, *517* (7535), 476−480.

(9) Saliba, M.; Matsui, T.; Seo, J.-Y.; Domanski, K.; Correa-Baena, J.-P.; Nazeeruddin, M. K.; Zakeeruddin, S. M.; Tress, W.; Abate, A.; Hagfeldt, A.; et al. Cesium-Containing Triple Cation Perovskite Solar Cells: Improved Stability, Reproducibility and High Efficiency. *Energy Environ. Sci.* **2016**, *9* (6), 1989−1997.

(10) Yi, C.; Luo, J.; Meloni, S.; Boziki, A.; Ashari-Astani, N.; Grätzel, C.; Zakeeruddin, S. M.; Röthlisberger, U.; Grätzel, M. Entropic Stabilization of Mixed A-cation $ABX_3$ Metal Halide Perovskites for High Performance Perovskite Solar Cells. *Energy Environ. Sci.* **2016**, *9* (2), 656−662.

(11) Li, J.; Shan, X.; Bade, S. G. R.; Geske, T.; Jiang, Q.; Yang, X.; Yu, Z. Single-Layer Halide Perovskite Light-Emitting Diodes with Sub-Band Gap Turn-on Voltage and High Brightness. *J. Phys. Chem. Lett.* **2016**, *7* (20), 4059−4066.

(12) Li, J.; Bade, S. G.; Shan, X.; Yu, Z. Single-Layer Light-Emitting Diodes Using Organometal Halide Perovskite/Poly(ethylene oxide) Composite Thin Films. *Adv. Mater.* **2015**, *27* (35), 5196−5202.

(13) Norris, D. J.; Efros, A. L.; Erwin, S. C. Doped Nanocrystals. *Science* **2008**, *319* (5871), 1776−1779.

(14) Guo, Y.; Liu, T.; Wang, N.; Luo, Q.; Lin, H.; Li, J.; Jiang, Q.; Wu, L.; Guo, Z. Ni-Doped $\alpha$-$Fe_2O_3$ as Electron Transporting Material for Planar Heterojunction Perovskite Solar Cells with Improved Efficiency, Reduced Hysteresis and Ultraviolet Stability. *Nano Energy* **2017**, *38*, 193−200.

(15) Abdelhady, A. L.; Saidaminov, M. I.; Murali, B.; Adinolfi, V.; Voznyy, O.; Katsiev, K.; Alarousu, E.; Comin, R.; Dursun, I.; Sinatra, L.; et al. Heterovalent Dopant Incorporation for Bandgap and Type Engineering of Perovskite Crystals. *J. Phys. Chem. Lett.* **2016**, *7* (2), 295−301.

(16) Wang, J. T.-W.; Wang, Z.; Pathak, S.; Zhang, W.; deQuilettes, D. W.; Wisnivesky-Rocca-Rivarola, F.; Huang, J.; Nayak, P. K.; Patel, J. B.; Yusof, H. A. M.; et al. Efficient Perovskite Solar Cells by Metal Ion Doping. *Energy Environ. Sci.* **2016**, *9* (9), 2892−2901.

(17) Zhang, J.; Shang, M.-h.; Wang, P.; Huang, X.; Xu, J.; Hu, Z.; Zhu, Y.; Han, L. n-Type Doping and Energy States Tuning in $CH_3NH_3Pb_{1-x}Sb_{2x/3}I_3$ Perovskite Solar Cells. *ACS Energy Lett.* **2016**, *1* (3), 535−541.

(18) Jiang, Q.; Chen, M.; Li, J.; Wang, M.; Zeng, X.; Besara, T.; Lu, J.; Xin, Y.; Shan, X.; Pan, B.; et al. Electrochemical Doping of Halide Perovskites with Ion Intercalation. *ACS Nano* **2017**, *11* (1), 1073−1079.

(19) Dawson, J. A.; Naylor, A. J.; Eames, C.; Roberts, M.; Zhang, W.; Snaith, H. J.; Bruce, P. G.; Islam, M. S. Mechanisms of Lithium Intercalation and Conversion Processes in Organic−Inorganic Halide Perovskites. *ACS Energy Lett.* **2017**, *2* (8), 1818−1824.

(20) Vicente, N.; Garcia-Belmonte, G. Methylammonium Lead Bromide Perovskite Battery Anodes Reversibly Host High Li-Ion Concentrations. *J. Phys. Chem. Lett.* **2017**, *8* (7), 1371−1374.

(21) Nguyen-Phan, T.-D.; Luo, S.; Vovchok, D.; Llorca, J.; Sallis, S.; Kattel, S.; Xu, W.; Piper, L. F. J.; Polyansky, D. E.; Senanayake, S. D.; et al. Three-Dimensional Ruthenium-Doped $TiO_2$ Sea Urchins for Enhanced Visible-Light-Responsive $H_2$ Production. *Phys. Chem. Chem. Phys.* **2016**, *18* (23), 15972−15979.

(22) Liu, G.; Yin, L.-C.; Wang, J.; Niu, P.; Zhen, C.; Xie, Y.; Cheng, H.-M. A Red Anatase $TiO_2$ Photocatalyst for Solar Energy Conversion. *Energy Environ. Sci.* **2012**, *5* (11), 9603−9610.

(23) Musico, Y. L. F.; Santos, C. M.; Dalida, M. L. P.; Rodrigues, D. F. Improved Removal of Lead (II) from Water Using a Polymer-Based Graphene Oxide Nanocomposite. *J. Mater. Chem. A* **2013**, *1* (11), 3789−3796.

(24) Wang, J.; Sun, Y.; Tian, M.; Liu, B.; Singh, M.; Chan, M. H. Superconductivity in Single Crystalline Pb Nanowires Contacted by




DOI: 10.1021/acsenergylett.7b01230
*ACS Energy Lett.* 2018, 3, 264−269

Normal Metal Electrodes. *Phys. Rev. B: Condens. Matter Mater. Phys.* **2012**, *86*, 035439.
(25) Zha, F. X.; Shao, J.; Jiang, J.; Yang, W. Y. "Blueshift" in Photoluminescence and Photovoltaic Spectroscopy of the Ion-Milling Formed *n*-on-*p* HgCdTe Photodiodes. *Appl. Phys. Lett.* **2007**, *90* (20), 201112.
(26) Begum, R.; Parida, M. R.; Abdelhady, A. L.; Murali, B.; Alyami, N. M.; Ahmed, G. H.; Hedhili, M. N.; Bakr, O. M.; Mohammed, O. F. Engineering Interfacial Charge Transfer in $CsPbBr_3$ Perovskite Nanocrystals by Heterovalent Doping. *J. Am. Chem. Soc.* **2017**, *139* (2), 731−737.
(27) Deng, Y.; Xiao, Z.; Huang, J. Light-Induced Self-Poling Effect on Organometal Trihalide Perovskite Solar Cells for Increased Device Efficiency and Stability. *Adv. Energy Mater.* **2015**, *5* (20), 1500721.
(28) deQuilettes, D. W.; Zhang, W.; Burlakov, V. M.; Graham, D. J.; Leijtens, T.; Osherov, A.; Bulović, V.; Snaith, H. J.; Ginger, D. S.; Stranks, S. D. Photo-Induced Halide Redistribution in Organic−Inorganic Perovskite Films. *Nat. Commun.* **2016**, *7*, 11683.
(29) Hoke, E. T.; Slotcavage, D. J.; Dohner, E. R.; Bowring, A. R.; Karunadasa, H. I.; McGehee, M. D. Reversible Photo-Induced Trap Formation in Mixed-Halide Hybrid Perovskites for Photovoltaics. *Chem. Sci.* **2015**, *6* (1), 613−617.
(30) Sutherland, B. R.; Johnston, A. K.; Ip, A. H.; Xu, J. X.; Adinolfi, V.; Kanjanaboos, P.; Sargent, E. H. Sensitive, Fast, and Stable Perovskite Photodetectors Exploiting Interface Engineering. *ACS Photonics* **2015**, *2* (8), 1117−1123.
(31) Lopatiuk, O.; Chernyak, L.; Osinsky, A.; Xie, J. Lithium-Related States as Deep Electron Traps in ZnO. *Appl. Phys. Lett.* **2005**, *87* (21), 214110.
(32) Yadav, H. K.; Gupta, V. A Comparative Study of Ultraviolet Photoconductivity Relaxation in Zinc Oxide (ZnO) Thin Films Deposited by Different Techniques. *J. Appl. Phys.* **2012**, *111* (10), 102809.
(33) Ma, Q.; Huang, S.; Wen, X.; Green, M. A.; Ho-Baillie, A. W. Y. Hole Transport Layer Free Inorganic $CsPbIBr_2$ Perovskite Solar Cell by Dual Source Thermal Evaporation. *Adv. Energy Mater.* **2016**, *6* (7), 1502202.
(34) Laban, W. A.; Etgar, L. Depleted Hole Conductor-Free Lead Halide Iodide Heterojunction Solar Cells. *Energy Environ. Sci.* **2013**, *6* (11), 3249−3253.



DOI: 10.1021/acsenergylett.7b01230
*ACS Energy Lett.* 2018, 3, 264−269